JOURNAL OF GEOPHYSICAL RESEARCH, VOL. 98, NO. A3, PAGES 4053–4061, MARCH 1, 1993

Siple Station, Antarctica, Experiments on Staircase Frequency Ramps as Approximations to Continuous Ramps

T. A. MIELKE AND R. A. HELLIWELL

Space, Telecommunications and Radioscience Laboratory, Stanford University, Stanford, California

VLF wave growth and emission triggering in the magnetosphere are known to depend on the coherence of the input signal. In these experiments the input signal may take the form of a constant frequency pulse (1 s duration) or a linearly chirped pulse (also 1 s duration) with a frequency ramp (1000 Hz/s) of either positive or negative slope. When a frequency ramp of 1000 Hz/s is approximated by a contiguous sequence of short, constant frequency steps, the growth behavior is unchanged for step durations less than 25 ms. For a step duration of 25 ms, the behavior more nearly resembles that of a pure ramp, but some evidence of individual step growth can be seen. For step durations of 50 ms and 100 ms, growth is relatively small and is confined to each individual step, with little coupling between steps. Rising ramps generally show more growth than falling ramps of similar step size and average slope, confirming earlier observations. An equivalent "sawtooth" frequency variation with an average slope of zero and a step size of 25 ms behaves much like a constant frequency pulse. An interpretation of the response to step size can be found in the theory of second-order resonance, where the spatial rates of change of the electron gyrofrequency and the Doppler-shifted wave frequency are equal. This theory also accounts for the previously observed "dot-dash" anomaly, where a long constant frequency pulse shows much more growth and emission triggering than a short pulse.

INTRODUCTION

Whistler mode waves injected at Siple Station, Antarctica, are often received at Roberval or Lake Mistissini, Quebec (near the north magnetic conjugate point), showing evidence of nonlinear amplification [*Carlson et al.*, 1985]. Such amplification is presumably due to interaction with energetic electrons in the magnetosphere. The process, sometimes called the coherent wave instability (CWI) [*Helliwell et al.*, 1980; *Carlson et al.*, 1990], is sketched in Figure 1. The detailed nature of this interaction is uncertain, but the data reported in this paper support previous suggestions that electron cyclotron resonance is the underlying mechanism. Earlier studies, assuming both cyclotron resonance and wave fields that are strong enough to cause particle trapping [*Dysthe*, 1971; *Nunn*, 1974; *Dowden et al.*, 1978], were able to reproduce some of the features of the CWI. More recent work [*Carlson et al.*, 1990] found wave amplification with cyclotron resonance even for signals much too weak to cause particle trapping. All of this previous work has been hampered by computing resources inadequate to fully simulate the wave-particle interaction, and by a paucity of in-situ data which could rigorously verify the consequent approximations. The experiment reported here was designed to test the cyclotron resonance hypothesis; it does not appear to provide any obvious test of the strong-versus-weak field controversy.

EXPERIMENTAL DATA

Data on the response of the magnetosphere to various rising frequency staircases are given in Figure 2, which shows dynamic spectra and amplitudes of both the Siple Station transmitter format and the signals as received at Lake Mistissini. The step durations used were 1 ms (equivalent to a 1-kHz/s frequency ramp), 10 ms, 25 ms, 50 ms, and 100 ms. Despite interference from atmospherics, two important features in the received signal are apparent. First, the received signal shows exponential amplitude growth (approximately 30-dB/s growth rate) up to a saturation level (about 25 dB) despite a constant amplitude transmitted signal on the first three frequency staircases. Second, on the first two staircases a free-running emission (visible on the received spectra) is triggered at pulse termination. The last (and coarsest) two staircases show little evidence of either exponential growth or emissions. It might be noted that the 10-ms and 25-ms staircases show lower growth rates than the 1-ms staircase. This may be due to progressively weaker wave-particle interactions for progressively coarser approximations to a frequency ramp.

Figure 3 (falling frequency staircases) shows essentially the same behavior as Figure 2. Growth and emissions are present on the first two staircases (1-ms and 10-ms step durations), and growth is present on the third staircase (25-ms step duration), but neither growth nor emissions are apparent on the last two (50-ms and 100-ms step durations), which are almost invisible in the spectra. Interference from sferics and emissions prevents determination of growth rates.

For step sizes greater than 50 ms a staircase appears to be too crude an approximation of a frequency ramp to exhibit the coherent wave instability. Comparison of Figures 2 and 3 shows that the major change from rising to falling frequency ramps is that saturated power is slightly reduced (about 20 dB versus 25 dB). Such moderate fluctuations in received power at Lake Mistissini are common and may relate to ionospheric absorption variations.

In Figure 4 (constant average frequency pulses) the rising and falling sawtooth pulses (made up of contiguous 25-ms-long 1-kHz/s frequency ramps) show only slightly less growth (27 dB and 24 dB, respectively) than the constant frequency pulse (30 dB), while all show similar emission triggering. The fact that the sawtooth pulses are about as good an approximation to the constant frequency pulse as the 25-ms staircases are to the frequency ramps is consistent with the previous data.

Figure 5 shows a diagnostic sequence (for monitoring propagation and growth) transmitted 50 s after the coherence experiment. This example illustrates the effect of pulse length on growth, first observed on Morse code signals and called the "dot-dash anomaly" [*Helliwell and Katsufrakis*, 1974; *Helliwell et al.*, 1964]. The 2-s-long constant frequency pulse shows growth and emission triggering, but the 200-ms-long constant frequency pulses show no

Paper number 92JA02562.
0148-0227/93/92JA-02562$02.00

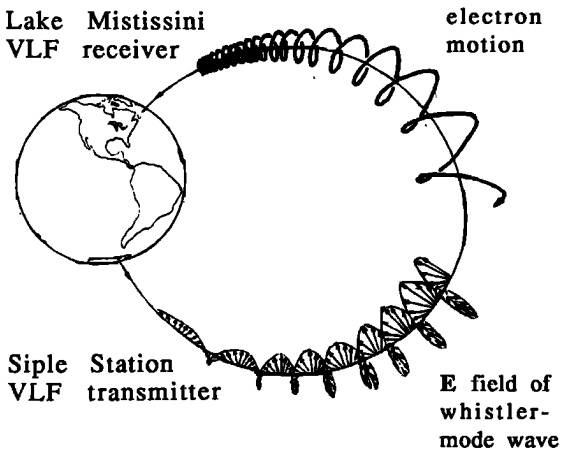

Fig. 1. Whistler mode wave and energetic electron.

triggering and much less growth. While the 200-ms pulses are staggered in time so as to form a staircase, examination of the received spectra clearly shows each step is independent of adjacent steps.

Second-Order Resonance Theory

It is commonly believed that wave growth comes about through interaction with energetic electrons in the magnetosphere. Both electron motion and whistler mode waves in the magnetosphere have characteristic helical structures, sketched in Figure 1. The axis of the electron helix follows a magnetic field line of the Earth, but that of the wave may deviate slightly. The pitch of the helix is a function of position on the magnetic field line. Where the wave and electron match in pitch, the electron sees a constant (rather than oscillating) electric field due to the wave, and at that location the strongest wave-particle interaction should occur. This condition corresponds to "first-order resonance". As Figure 1 shows, the helix described by electron motion stretches along the axis as the electron approaches the equator. Conversely, the helix described by the whistler mode wave becomes compressed as the wave approaches the equator. Thus, the length of magnetic field line over which strong interaction occurs will depend on how rapidly the two helices diverge in pitch. A measure of the length over which strong interaction takes place can be obtained from the "second-order resonance" condition, the derivation of which is straightforward.

At location s_0 on a magnetic field line of the Earth, an electron moving along the field line with a velocity $v_\parallel$ encounters a ducted whistler mode wave at a frequency f and phase velocity v_p. In a reference frame moving along the field line at $v_\parallel$ the electron executes a circular motion at the local gyrofrequency f_H while the electric field of the whistler mode wave executes a circular motion at the Doppler-shifted wave frequency $f' = f(1 + v_\parallel/v_p)$. With s being distance along the field line in the direction of $v_\parallel$, the gyrofrequency and Doppler-shifted wave frequency can each be expanded in a Taylor series:

$$f_H(s) = f_H|_{s_0} + \frac{df_H}{ds}|_{s_0}\Delta s + \frac{1}{2}\frac{d^2 f_H}{ds^2}|_{s_0}\Delta s^2 + \dots \quad (1)$$

$$f'(s) = f'|_{s_0} + \frac{df'}{ds}|_{s_0}\Delta s + \frac{1}{2}\frac{d^2 f'}{ds^2}|_{s_0}\Delta s^2 + \dots \quad (2)$$

For first-order resonance the first terms of the two Taylor series are equal; for second-order resonance the second terms of the two Taylor series are also equal.

The phase deviation over a distance Δs between the perpendicular velocity $v_\perp$ of the resonant electron and the electric field of the wave can be expressed as

$$\theta = \int_0^{\Delta s} \frac{2\pi}{v_\parallel}(f_H(s) - f'(s))ds \quad (3)$$

When this phase deviation reaches $\pi/2$ the coherent interaction between electron and wave is considered to end. Twice Δs is designated the "interaction length" l_i [*Helliwell*, 1967]. A short interaction length should lead to a weak interaction, and a long interaction length to an extended and therefore strong interaction, all else being equal.

Another quantity of interest is the length of field line along which the electron encounters a wave pulse of duration τ. This "encounter length" might be greater than or less than the interaction length depending on pulse duration. A short pulse, with a correspondingly short encounter length, is expected to interact only weakly with the electron. Where v_g is the wave group velocity, this encounter length l_e is given by

$$l_e = \frac{\tau}{1/v_\parallel + 1/v_g} \quad (4)$$

If the transmitted pulse is a frequency staircase or sawtooth instead of a frequency ramp or constant frequency pulse, the instantaneous phase deviation θ_i (relative to a resonant ramp or constant frequency pulse of the same average df/dt) will depend on the step length. If θ_i is small, the staircase or sawtooth should behave like a slightly perturbed resonant pulse. The quantity θ_i can be calculated from the expression for θ, using the instantaneous rather than the average pulse frequency.

Analytic Formulas

An analytical form for second-order resonance and interaction lengths, applicable at or very near the equator, was developed in the paper which introduced the second-order resonance concept [*Helliwell*, 1967, 1970]. Numerical modeling has been used to examine some aspects of the theory (but not interaction lengths) over a wide range of electron pitch angles and magnetic latitudes at an L shell of 4.5 [*Carlson et al.*, 1985]. This section presents extended analytic results useful within about 10° of the equator.

For a dipole field model and a nonrelativistic electron [*Roederer*, 1970; *Helliwell*, 1965], the gyrofrequency f_H, equatorial gyrofrequency $f_{H_{eq}}$, equatorial plasma frequency $f_{p_{eq}}$, electron pitch angle α, group velocity v_g, and phase velocity v_p (for a wave propagating parallel to B_0) are given by

$$f_H(\phi) = f_{H_{eq}}\frac{(4 - 3\cos^2\phi)^{1/2}}{\cos^6\phi} \quad (5)$$

$$f_{H_{eq}} = \frac{873.6}{L^3}\ \text{kHz} \quad (6)$$

$$f_{p_{eq}} = 8.9775\sqrt{n_{eq}}\ \text{kHz with electron density } n_{eq} \text{ in cm}^{-3} \quad (7)$$

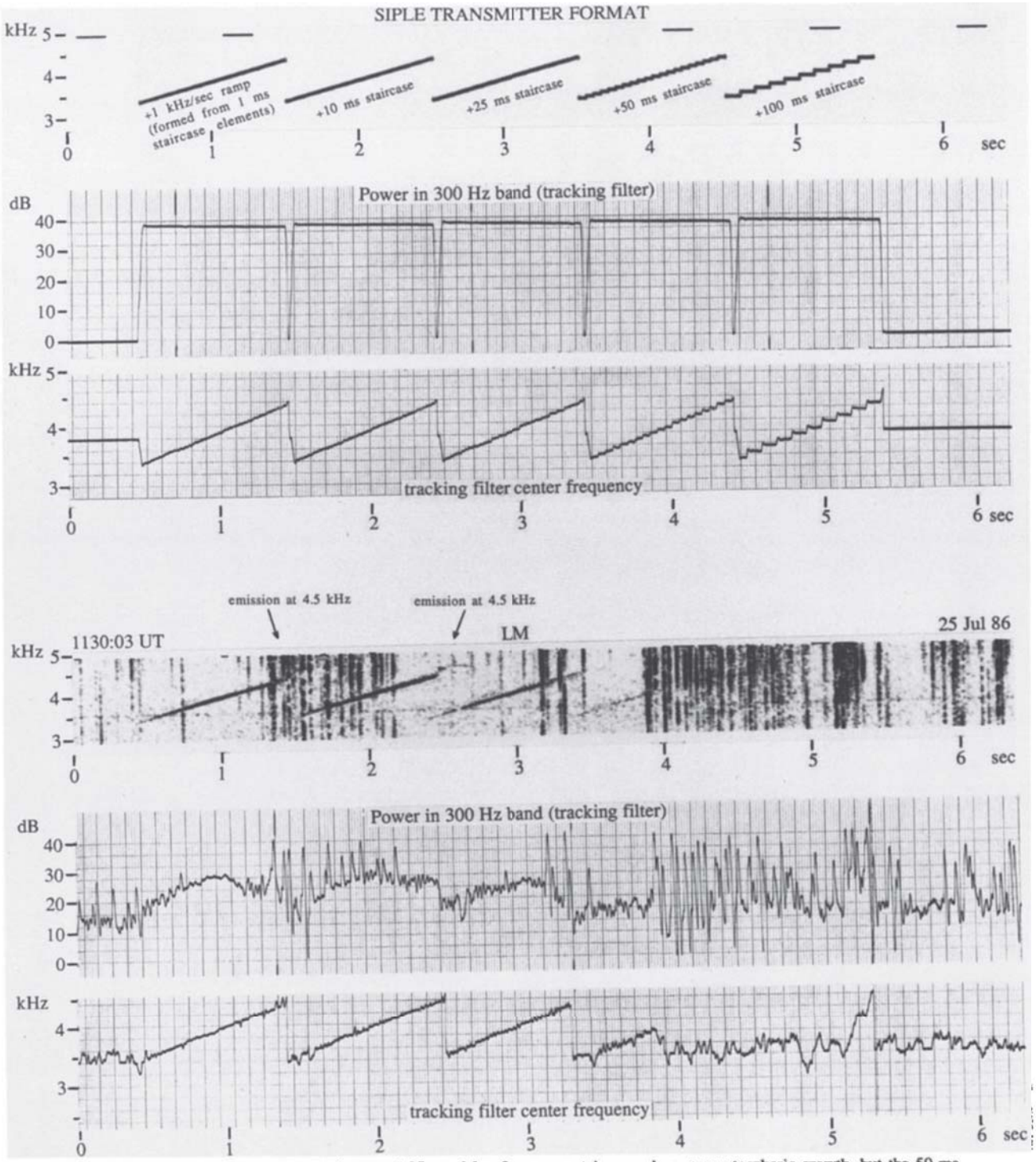

Fig. 2. The rising frequency ramp, 10-ms, and 25-ms rising frequency staircases show magnetospheric growth, but the 50-ms staircase and 100-ms staircase do not. Note that on this and subsequent spectra the frequency resolution is 20 Hz, so only the 50-ms and 100-ms staircase steps are clearly resolved. The 200-ms constant frequency pulses at 5 kHz provide timing data. Spectral intensity is indicated by a gray scale. For the power charts the tracking filter adjusts the center of the passband to follow the slowly varying carrier frequency. The spikes in the tracking filter output are caused by sferics.

$$\sin^2 \alpha = \frac{f_H}{f_{H_{eq}}} \sin^2 \alpha_{eq} \tag{8}$$

$$v_p = c \frac{f_H}{f_p} \Lambda^{1/2} (1 - \Lambda)^{1/2} \tag{9}$$

$$v_g = 2c \frac{f_H}{f_p} \Lambda^{1/2} (1 - \Lambda)^{3/2} \tag{10}$$

where $\Lambda = f/f_H$ and α_{eq} is the equatorial pitch angle.

Within about 10° of the geomagnetic equator the plasma frequency f_p can be taken as constant [*Park*, 1972], and reasonably simple forms of the Taylor series can be obtained. The results presented here also assume that the wave frequency varies linearly with time. The value of df/dt will vary with position along the propagation path due to dispersion, but the variation of frequency with time is assumed to remain linear. At

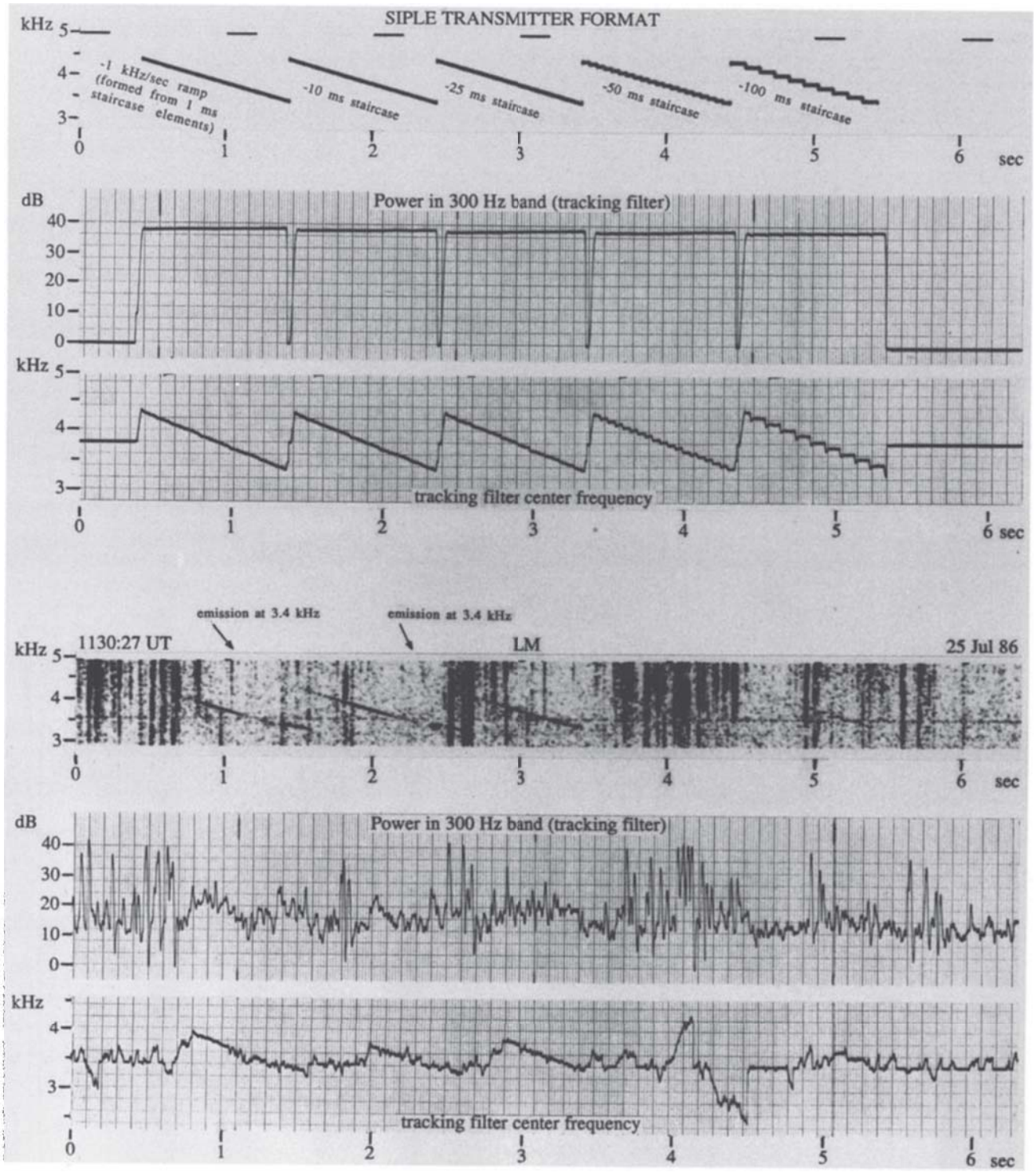

Fig. 3. The falling frequency ramp, 10-ms, and 25-ms falling frequency staircases show magnetospheric growth, but the 50-ms staircase and 100-ms staircase do not. (The 100-ms staircase appears to act as a sequence of independent CW pulses.)

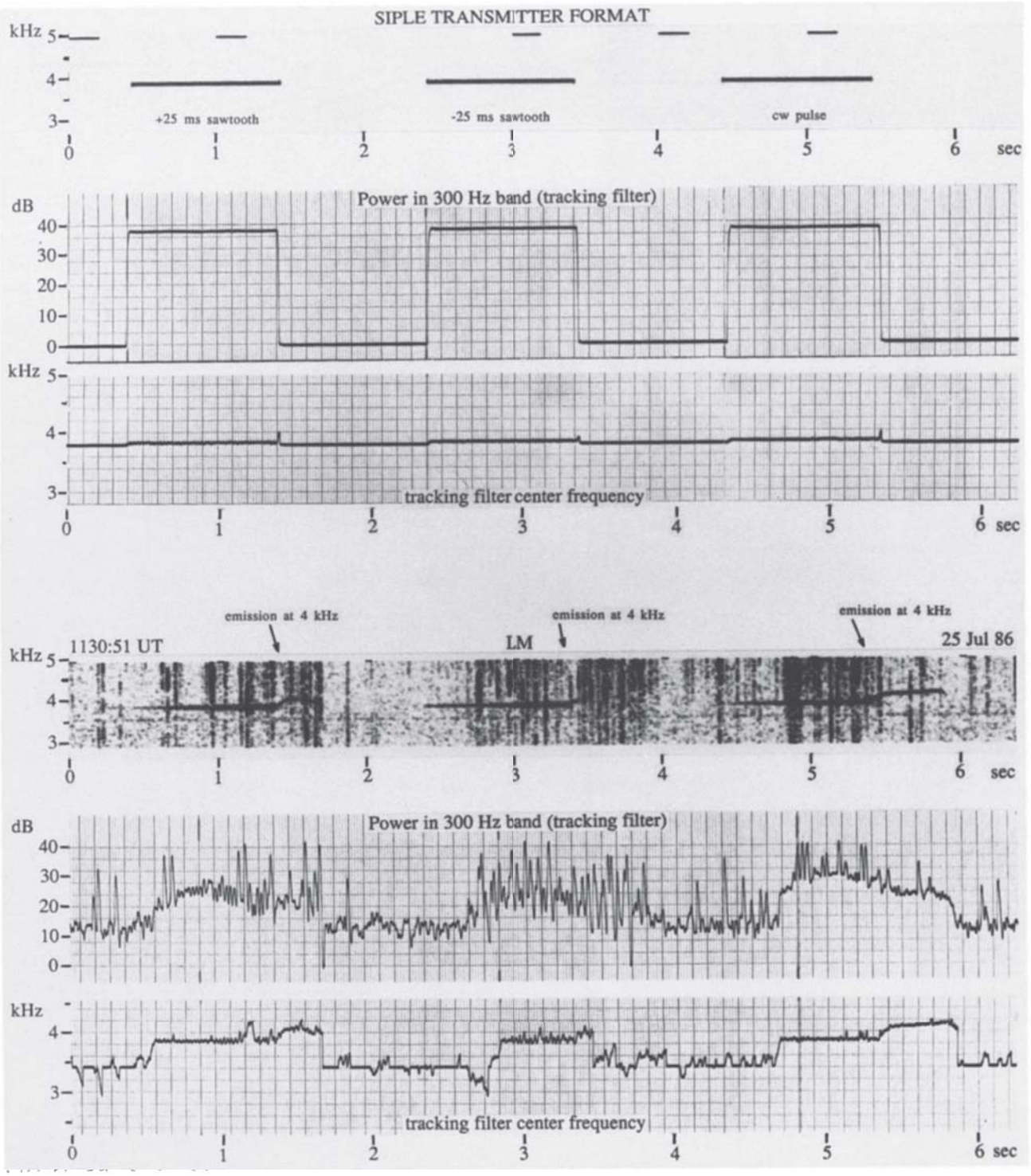

Fig. 4. The +25-ms sawtooth, −25-ms sawtooth, and CW pulses all show magnetospheric growth.

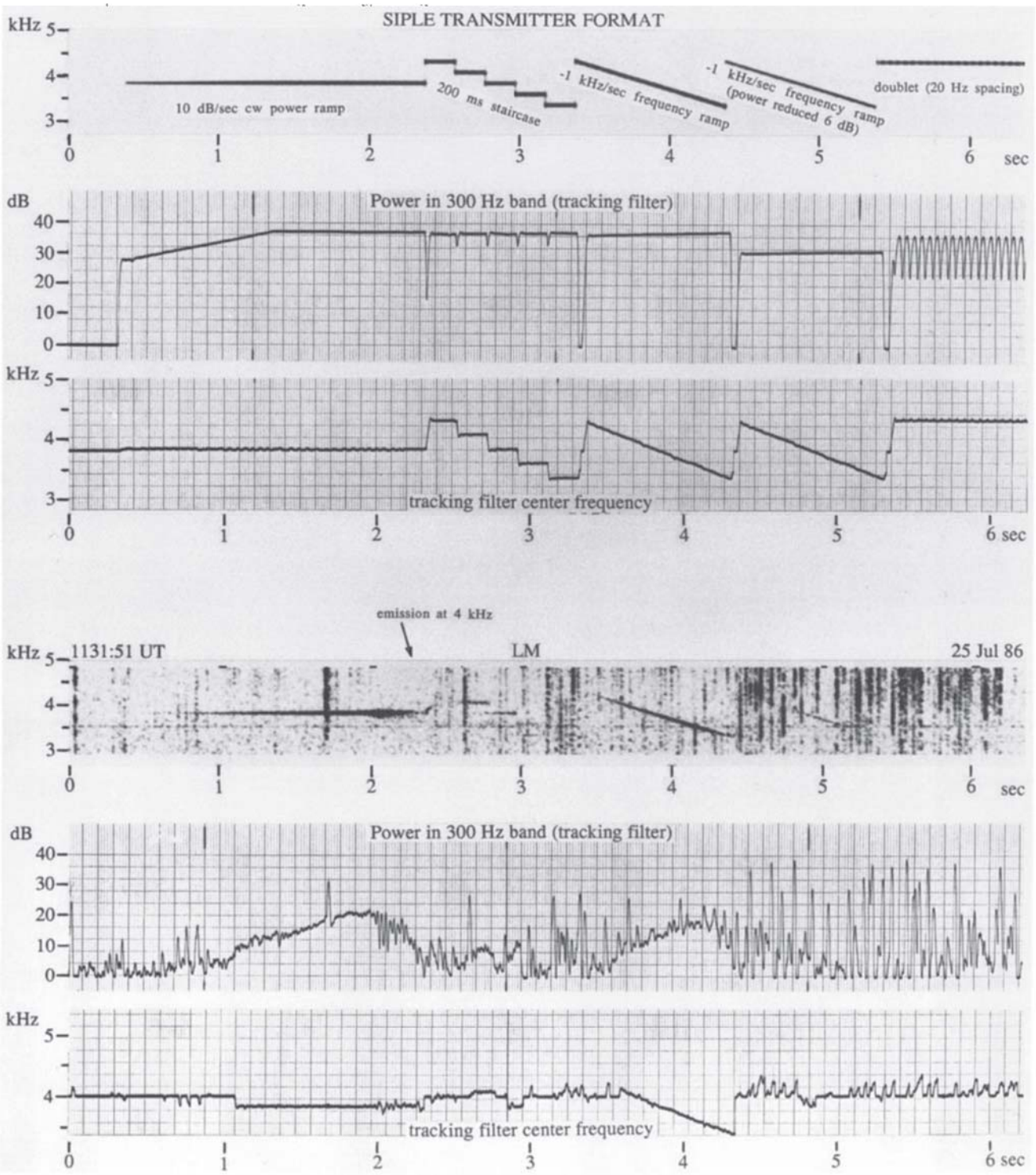

Fig. 5. Example of the "dot-dash anomaly". The CW power ramp and the −1-kHz/s frequency ramp both grow and reach saturation. The reduced power frequency ramp is below threshold and does not grow. Only the second and third 200-ms steps in the frequency staircase can be identified. Both show growth but do not reach saturation.

$L \approx 4.5$ and $df/dt \approx 1$ kHz/s (the conditions of the Stair Coherence experiment, abbreviated STACO) this is reasonable. For $df/dt \geq 10$ kHz/s, dispersion introduces significent curvature, and a more complicated analysis is required. The formulas for df'/ds and d^2f'/ds^2 make use of the first-order resonance condition $f' = f_H$ to simplify the algebra but do not specify any other implicit relationship. With these caveats we obtain

$$\frac{df_H}{ds} = -f_H \frac{3 \sin\phi(8 - 5\cos^2\phi)}{R_{eq} \cos\phi(4 - 3\cos^2\phi)} \tag{11}$$

$$\frac{d^2 f_H}{ds^2} = f_H \frac{3(3 + 36\sin^2\phi + 118\sin^4\phi + 75\sin^6\phi)}{R_{eq}^2(1 + 3\sin^2\phi)^2} \tag{12}$$

with $R_{eq} = LR_E = L(6371 \text{ km})$, and

$$\frac{df'}{ds} = \frac{df}{dt}\frac{(1+2\Lambda)^2}{4v_p\Lambda(1-\Lambda)} - \frac{df_H}{ds}\frac{1+(1-\Lambda)\tan^2\alpha}{2} \tag{13}$$

$$\begin{aligned}\frac{d^2 f'}{ds^2} = &-\frac{d^2 f_H}{ds^2}\frac{1+(1-\Lambda)\tan^2\alpha}{2} \\ &+ \left(\frac{df_H}{ds}\right)^2 \frac{4-[1-(1-\Lambda)\tan^2\alpha]^2}{4f_H(1-\Lambda)} \\ &- \frac{df_H}{ds}\frac{df}{dt}\frac{(1+2\Lambda)[3(1+2\Lambda)+2(1-\Lambda)^2\tan^2\alpha]}{8f_H v_p \Lambda(1-\Lambda)^2} \\ &+ \left(\frac{df}{dt}\right)^2 \frac{(1+2\Lambda)^2(1-4\Lambda)}{16 f_H v_p^2 \Lambda^2(1-\Lambda)^3}\end{aligned} \tag{14}$$

Dispersion will alter the slope of a transmitted frequency ramp. To calculate this effect, the group delay from Siple Station to the equator (Δt_{eq}) [*Bernard*, 1973] is differentiated with respect to frequency. Within about 10° of the equator, propagation over an additional distance s from the equator introduces an additional group delay (Δt_s) which is also differentiated with respect to frequency. The resulting slope changes are

$$\begin{aligned}\frac{d(\Delta t_{eq})}{df} = &\frac{t_n}{8(f/f_n)^{1/2} f_n (1-\Lambda_n f/f_n)^2} \times \\ &[(1+\Lambda_n)(3\Lambda_n - f_n/f) - (3\Lambda_n - 1)(1+\Lambda_n f/f_n)]\end{aligned} \tag{15}$$

where $\Lambda_n = f_n/f_{H_{eq}}$ with f_n denoting nose frequency and t_n denoting nose delay, and

$$\begin{aligned}\frac{d(\Delta t_s)}{df} = &\frac{f_{p_{eq}} R_{eq}\phi}{4cf^{3/2} f_{H_{eq}}^{1/2}(1-f/f_{H_{eq}})^{5/2}} \times \\ &\left[-1 + 4f/f_{H_{eq}} + \frac{3}{4}\phi^2 \frac{1 - 8f/f_{H_{eq}} - 8(f/f_{H_{eq}})^2}{1 - f/f_{H_{eq}}}\right]\end{aligned} \tag{16}$$

The slope of a transmitted frequency ramp at a location s is then given by

$$\frac{df}{dt} = \left[\frac{d(\Delta t_{eq})}{df} + \frac{d(\Delta t_s)}{df} + \frac{1}{M_{TX}}\right]^{-1} \tag{17}$$

where $M_{TX} = df/dt$ at the transmitter.

At a location s, application of the second-order resonance condition $df'/ds = df_H/ds$ requires a choice of electron pitch angle α. The second-order resonance condition is not very sensitive to electron pitch angle for $\alpha \leq 45°$. Accordingly, loss cone electrons were selected in order to minimize assumptions about the electron distribution function. The magnetosphere contains a diverse population of energetic particles. This leads to a theorem which might be phrased as "anything you want will be there". In this case, electrons slightly more energetic than the resonant electrons are expected to give up energy to the wave and provide growth while slightly less energetic electrons are expected to be accelerated by the wave and produce damping. Electrons far from resonance should interact only weakly with the wave and can be neglected. An unfortunate corollary to the above theorem might be stated "all the stuff you don't want will be there too"; thus as lower energy electrons are typically more numerous than higher energy electrons, damping should be expected. A way out of this difficulty is to select resonant electrons at the loss cone, assumed to be empty. In that case for a given resonant $v_\parallel$, only electrons with $v_\perp$ greater than that of the resonant electrons will be present. Thus the resonant electrons are taken to have pitch angles given by [*Roederer*, 1970]

$$\sin^2\alpha_{eq} = \frac{1}{L^3\sqrt{4 - 3/L}} \tag{18}$$

An alternative wave-particle interaction mechanism is possible between a costreaming electron and the whistler mode wave when the electron $v_\parallel$ equals wave phase velocity v_p (Landau resonance) [*Brice*, 1960]. Here again the electron sees an essentially constant field, and if a longitudinal wave E field exists (which is to be expected in a ducted whistler mode wave, analogous to light propagation in a fiber-optic cable) a strong interaction can occur. As $v_\parallel$ is greatest at the equator (a dipole field is assumed) while v_p is minimum there, such a costreaming interaction can occur over only a limited region. By expressing both v_p and $v_\parallel$ in Taylor series and matching terms in the respective series one can estimate the location and extent of the interaction region in a manner analogous to that used for the gyroresonance case. An important difference between the longitudinal and gyroresonance cases is that gyroresonance places far more stringent restrictions on wave coherence. The gyroresonant (counterstreaming) electron "sees" hundreds of cycles of the wave as it traverses its interaction region, and if wave coherence fails then the interaction is prematurely ended. In contrast, the Landau resonant (costreaming) electron "sees" only a single point of the wave. The length of the interaction region can in fact be defined by those locations at which the electron has "slipped" relative to the wave by a quarter wavelength ($\pm\lambda/4$). In the Landau resonance case therefore staircase step length and pulse length (for steps and pulses longer than one wavelength) are unimportant to the interaction. Since the "dot-dash anomaly" shows experimentally that pulse length is important in the coherent wave instability, Landau resonance is presumably not the cause.

Comparison of Data and Theory

The STACO format (a variety of constant frequency pulses, linear frequency ramps, frequency staircases, and frequency sawtooth pulses) was transmitted from Siple Station, Antarctica, and received at Lake Mistissini (near Roberval, Quebec) on July 25, 1986. It provides an excellent test of the first- and second-order resonance concepts. Measurements of frequency and time delay of the received signal [*Ho and Bernard*, 1973], combined with a diffusive equilibrium magnetospheric model [*Park*, 1972], yielded the propagation parameters L shell = 4.5 and n_{eq} = 530 cm^{-3}. With these parameters and the transmitted signal characteristics (f = 3.8 kHz and df/dt = +1 kHz/s, -1 kHz/s, or 0 kHz/s) it was possible to determine the second-order resonance locations. Loss cone electrons were assumed. The regions of second-order resonance were located at the geomagnetic latitudes of −5.684° for the +1-kHz/s ramps, +6.005° for the −1-kHz/s ramps, and 0° for the constant frequency pulses. Interaction lengths l_i were calculated to be about 900 km, while the encounter length l_e for a 1-s pulse was calculated to be about 5000 km. This prediction of strong interaction between coherent whistler mode waves and energetic electrons fits with the growth and emissions seen on the

frequency ramps and constant frequency pulse.

Encounter lengths were also calculated for the individual steps of the frequency staircases and sawtooth pulses. The greatest step encounter length was 460 km for the 100-ms staircase pulse (Figures 2 and 3), considerably less than the interaction length. This suggests weak wave-particle interaction for a single isolated step even for the longest steps. In the data the 100-ms steps do not seem to be coupled to adjacent steps and are also much weaker than the 1-s pulses.

For the 200-ms pulse in the diagnostic sequence (Figure 5) the encounter length is about equal to the interaction length. It would appear that an encounter length somewhat greater than the interaction length is required to produce growth to saturation and emission triggering. Based on extrapolation of the observed growth rate and on the saturated power level of the 2-s pulse, the required ratio of encounter length to interaction length is around 2–3, corresponding in this instance to a 400–600 ms pulse length. These data are summarized in Table 1.

Examination of the instantaneous phase deviation of the 50-ms and greater staircase pulses gives a reason for the uncoupling of adjacent steps. The maximum instantaneous phase deviation was calculated for all frequency staircases and sawtooth pulses. For steps of 1, 10, 25, 50, and 100 ms the corresponding maximum θ_i were 0.0003π, 0.03π, 0.17π, 0.67π, and 2.7π respectively. As these data show, maximum θ_i exceeded $\pi/2$ only for the 50-ms and 100-ms staircases. These staircases are therefore expected to show weak interactions with energetic electrons and indeed are much weaker than the other pulses when received at Lake Mistissini. These data are summarized in Table 2.

In the cases shown in Figures 2, 3, 4, and 5 (July 25, 1986, 1130–1132 UT) the second-order resonance theory explains why the rising frequency ramps, rising frequency staircases with modest step length, falling frequency ramps, falling frequency staircases with modest step length, sawtooth, and constant frequency pulses transmitted from Siple Station all showed similar magnetospheric growth. It also explains why the coarser frequency staircases showed little magnetospheric growth. Frequently, however, behavior such as that of Figure 6 (October 8, 1986, 1147–1148

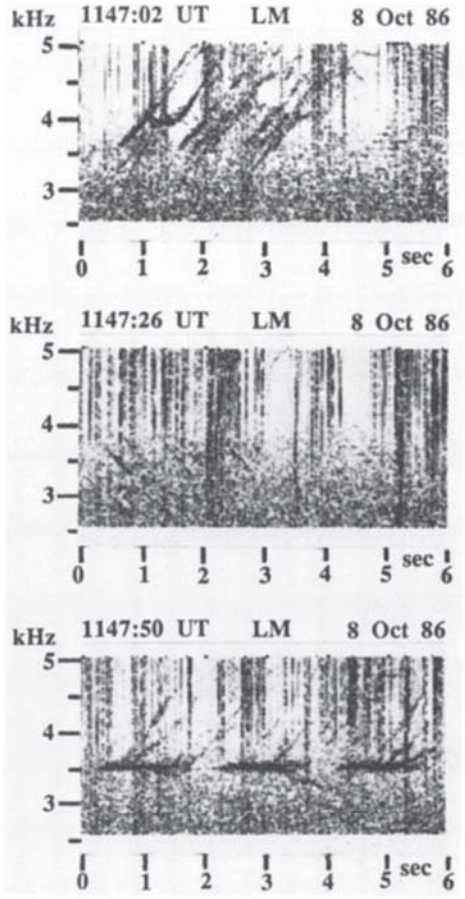

Fig. 6. The rising frequency staircases (2.98 kHz to 3.98 kHz) with step durations less than 50 ms (top panel, like those of Figure 2) show growth and emissions on at least three paths. The constant frequency pulses (3.48 kHz) and 25-ms sawtooth pulses (bottom panel, like those of Figure 4) also show growth and emissions on multiple paths (the multiplicity of paths causes the extension of the received pulse length). Falling frequency staircases (3.98 kHz to 2.98 kHz) (middle panel, like those of Figure 3) show less growth.

TABLE 1. Interaction Lengths and Encounter Lengths for CW Pulses

Signal	Interaction Length l_i, km	Encounter Length l_e, km	l_e/l_i	Observations
2-s CW power ramp	920	9200	9200/920 = 10	growth and triggering (Figure 5)
1-s CW pulse	920	4600	4600/920 = 5	growth and triggering (Figure 4)
200-ms CW pulse	920	920	920/920 = 1	growth, no triggering (Figure 5)
100-ms CW pulse	920	460	460/920 = 1/2	no apparent growth (Figures 2, 3)
50-ms CW pulse	920	230	230/920 = 1/4	no apparent growth (Figures 2, 3)

TABLE 2. Phase Deviations of Frequency Staircases Relative to a Resonant Frequency Ramp

Signal	Maximum Instantaneous Phase Deviation θ_i	$\theta_i/(\pi/2)$	Observations
1-ms stair	$0.0003\pi = 0.05°$	0.0006	growth and triggering (Figures 2, 3, 5)
10-ms stair	$0.03\pi = 5.4°$	0.06	growth and triggering (Figures 2, 3)
25-ms stair	$0.17\pi = 30°$	0.34	growth, no triggering (Figures 2, 3)
50-ms stair	$0.67\pi = 120°$	1.34	no apparent growth (Figures 2, 3)
100-ms stair	$2.7\pi = 490°$	5.4	no apparent growth (Figures 2, 3)

UT) is seen. Here the constant frequency pulses and rising frequency ramps show much stronger magnetospheric growth than the falling frequency ramps. Second-order resonance theory predicts near symmetry for rising and falling frequency ramps. Reasons for the observed preferential magnetospheric growth of rising frequency ramps versus falling frequency ramps are not clear. Factors that may be important in this connection, but are outside the scope of this paper, are the effect of the actual $f(t)$ shape of the ramp in the interaction region and the variation of the temporal growth rate with frequency that could affect the relative overall growth of rising and falling ramps.

CONCLUSION

Experimental evidence supports identification of the electron cyclotron interaction as the underlying process for nonlinear wave growth and emission triggering in the magnetosphere. Based on this wave-particle interaction, second-order resonance theory predicts the observed relative growth of coarse versus fine frequency staircases. It also predicts the observed relative growth of short versus long constant frequency pulses ("dot-dash anomaly"). An additional feature of the experimental data is that rising frequency ramps often grow more than falling frequency ramps. A theoretical explanation of this preference for rising ramps is not yet available.

Acknowledgments. We thank John Katsufrakis for management of the field programs in which the STACO data were acquired, and Jim Logan for his service at Siple Station operating the transmitter. The contributions of Jerry Yarbrough in data analysis are also greatly appreciated. Reviewers' comments were helpful and appreciated. This research was supported by National Science Foundation under grants DPP 86-13783 and DPP 89-18326.

The Editor thanks M. Hayakawa and H. C. Koons for their assistance in evaluating this paper.

REFERENCES

Bernard, L. C., A new nose extension method for whistlers, *J. Atmos. Terr. Phys.*, *35*, 871–880, 1973.

Brice, N. M., Traveling wave amplification of whistlers, *J. Geophys. Res.*, *65*, 3840–3842, 1960.

Carlson, C. R., R. A. Helliwell and D. L. Carpenter, Variable frequency VLF signals in the magnetosphere: Associated phenomena and plasma diagnostics, *J. Geophys. Res.*, *90*, 1507–1521, 1985.

Carlson, C. R., R. A. Helliwell and U. S. Inan, Space-time evolution of whistler-mode wave growth in the magnetosphere, *J. Geophys. Res.*, *95*, 15073–15089, 1990.

Dowden, R. L., A. D. McKay and L. E. S. Amon, Linear and nonlinear amplification in the magnetosphere during a 6.6-kHz transmission, *J. Geophys. Res.*, *83*, 169–181, 1978.

Dysthe, K. B., Some studies of triggered whistler emissions, *J. Geophys. Res.*, *76*, 6915–6931, 1971.

Helliwell, R. A., *Whistlers and Related Ionospheric Phenomena*, pp 23–32, 317–321, Stanford University Press, Stanford, Calif., 1965.

Helliwell, R. A., A theory of discrete VLF emissions from the magnetosphere, *J. Geophys. Res.*, *72*, 4773–4790, 1967.

Helliwell, R. A., Intensity of discrete VLF emissions, in *Particles and Fields in the Magnetosphere*, edited by B. M. McCormac, pp 292–301, D. Reidel, Norwell, Mass., 1970.

Helliwell, R. A., and J. P. Katsufrakis, VLF wave injection into the magnetosphere from Siple Station, Antarctica, *J. Geophys. Res.*, *79*, 2511–2518, 1974.

Helliwell, R. A., J. Katsufrakis, M. Trimpi, and N. Brice, Artifically stimulated very-low-frequency radiation from the ionosphere, *J. Geophys. Res.*, *69*, 2391–2394, 1964.

Helliwell, R. A., D. L. Carpenter and T. R. Miller, Power threshold for growth of coherent VLF signals in the magnetosphere, *J. Geophys. Res.*, *85*, 3360–3366, 1980.

Ho, D. and L. C. Bernard, A fast method to determine the nose frequency and minimum group delay of a whistler when the causative spheric is unknown, *J. Atmos. Terr. Phys.*, *35*, 881–887, 1973.

Nunn, D., A self-consistent theory of triggered VLF emissions, *Planet. Space Sci.*, *22*, 349–378, 1974.

Park, C. G., Methods of determining electron concentrations in the magnetosphere from nose whistlers, *Tech. Rep. 3454-1*, p. 52, Radiosci. Lab., Stanford Electron. Lab., Stanford Univ., Stanford, Calif., 1972.

Roederer, J. G., *Dynamics of Geomagnetically Trapped Radiation*, pp 34, 52–55, Springer-Verlag, New York, 1970.

R. A. Helliwell and T. A. Mielke, STAR Laboratory, Stanford University,Stanford, CA 94305.

(Received May 19, 1992;
revised October 12, 1992;
accepted October 12, 1992.)